Talanta 134 (2015) 206–214

Contents lists available at ScienceDirect

Talanta

journal homepage: www.elsevier.com/locate/talanta

Copper–zinc alloy nanoparticle based enzyme-free superoxide radical sensing on a screen-printed electrode

Burak Derkus, Emel Emregul*, Kaan C. Emregul

Ankara University, Science Faculty, Department of Chemistry, Tandoğan, Ankara 06100, Turkey

ARTICLE INFO

Article history:
Received 11 August 2014
Received in revised form
29 October 2014
Accepted 2 November 2014
Available online 18 November 2014

Keywords:
Superoxide dismutase
Enzyme-free biosensor
Screen-printed electrode
CuZn nanoparticles
Nanobiosenosors

ABSTRACT

In this paper, amperometric enzyme-free sensors using superoxide dismutase (SOD) enzyme as a catalyst for the dismutation reaction of superoxides into oxygen and hydrogen peroxide, enabling superoxide radical detection have been described. For this purpose, the surfaces of screen-printed platinum electrodes have been modified with gelatin composites of CuO, ZnO and CuZn nanoparticles with the expectation of an increase in catalytic effect toward the dismutation reaction. SOD containing electrodes were also prepared for comparative studies in which glutaraldehyde was used as a cross-linker for the immobilization of SOD to the nanocomposite materials. Electrochemical measurements were carried out using a screen-printed electrochemical system that included potassiumferrocyanide ($K_4[Fe(CN)_6]$) and potassiumferricyanide ($K_3[Fe(CN)_6]$) as the redox probes. The results revealed that the enzyme-free detection method using CuZn nanoparticles can determine superoxide radicals with high performance compared to other detection methods prepared with different nanoparticles by mimicking the active region of superoxide dismutase enzyme. The anodic (ks_a) and cathodic (ks_c) electron transfer rate constants and the anodic (α_a) and cathodic (α_c) transfer coefficients were evaluated and found to be $ks_a=6.31\ s^{-1}$ and $\alpha_a=0.81$, $ks_c=1.48\ s^{-1}$ and $\alpha_c=0.19$ for the gelatin–CuZn–SOD electrode; $ks_a=6.15\ s^{-1}$ and $\alpha_a=0.79$, $ks_c=1{,}63\ s^{-1}$ and $\alpha_c=0.21$ for the enzyme-free gelatin–CuZn electrode. The enzyme-free electrode showed nearly 80% amperometric performance with respect to the enzyme containing electrode indicating the superior functionality of enzyme-free electrode for the detection of superoxide radicals.

1. Introduction

Due to its overwhelming reaction rate owing to a radical mechanism and high specificity [1], the superoxide dismutase (SOD) enzyme offers a great potential for sensitive quantification of superoxide radicals in various biological samples especially in cancerous tissues using biosensing technology. Superoxide radicals ($O_2^{\bullet -}$) are known to damage some biological molecules [2–4] and signal pathways, and also play important roles in heart disease [5], cancer [6] and neuronal dejeneration [7]. Hence, the study of superoxide radicals has attracted considerable attention in recent years. SODs are metalloenzymes which have iron (Fe), manganese (Mn), nickel (Ni), or copper–zinc (CuZn) ions in their active region that catalyze the dismutation of superoxide to oxygen and hydrogen peroxide [8].

Copper–zinc superoxide dismutase is present in the cytosol, nucleus, peroxisomes, and mitochondrial intermembrane space of human cells, acting as an antioxidant enzyme by lowering the steady-state concentration of superoxide. The human enzyme is a 32-kDa homodimer, with a copper- and zinc-binding site each per 153-amino acid subunits [9–11]. The copper site is the heart of the enzymatic active site where SOD1 protein catalyzes the disproportionation of superoxide to give dioxygen and hydrogen peroxide. This catalysis is a two-step process: one molecule of superoxide first reduces the cupric ion to form dioxygen and then a second molecule of $O_2^{\bullet -}$ reoxidizes the cuprous ion to form hydrogen peroxide. Detailed information about the catalyzer effect of CuZn can be found in literature [12].

The dismutation of superoxide proceeds via a two-step reaction if the enzyme includes CuZn [13]:

$$O^{2-} + Cu(II)ZnSOD \rightarrow O_2 + Cu(I)ZnSOD$$

$$O^{2-} + Cu(I)ZnSOD + 2H^+ \rightarrow H_2O_2 + Cu(II)ZnSOD$$

The overall reaction is

$$O^{2-} + 2H^+ \rightarrow H_2O_2 + O_2$$

This reaction is often used to determine the superoxide anion. In order to understand the role of $O_2^{\bullet -}$ in pathology and physiology and the relationship between $O_2^{\bullet -}$ and environmental stresses,

* Corresponding author. Tel.: +90 312 212 60 40.
E-mail address: eemregul@yahoo.com (E. Emregul).

http://dx.doi.org/10.1016/j.talanta.2014.11.003
0039-9140/

it is essential to determine $O_2^{\bullet -}$ in a variety of in vitro and in vivo models. Due to its low concentration, high reactivity, and short lifetime, it is still an analytical challenge to detect the local concentration of $O_2^{\bullet -}$, especially in biological systems. Determination of free radicals is usually carried out with spectrometry, fluorometry, chemiluminensence, and electron spin resonance [14–16]. Recent attempts have concentrated on electrochemical methods due to their direct, real-time measurements and capability for in vivo detection [17–19].

Recently the combination of nanomaterials with biological agents has provided a novel way for the fabrication of diagnostic tools. Oxide nanoparticles like zinc oxide (ZnO), tin oxide (SnO), copper oxide (CuO) and titanium dioxide (TiO_2) are often used to immobilize biomolecules due to their biocompatibility. CuO is a semiconductor nanoparticle with 1.2 eV band-gap which has many applications such as the fabrication of electrochemical biosensors [20], optical and photovoltaic devices [21], heterogeneous catalysis [22], anode materials for lithium-ion batteries [23] and enzyme-free glucose biosensor [24]. Various shapes of CuO have been produced such as nanowires [25], nanorods [26], nano-flowers [27], and nanoellipsoids [28]. One of the interesting metal oxide nanoparticles which has amazing properties is ZnO nanoparticles. ZnO has an isoelectric point of 9.5, which is quite high compared with other nanoparticles [29]. At biological pH values, proteins with a low isoelectric point can be immobilized on positively charged ZnO nanoparticle surfaces via electrostatic forces [30]. ZnO nanoparticles are also nontoxic, have good biocompatibility and high stability. All these properties make ZnO nanoparticles ideal materials for biosensing applications.

Screen-printed electrodes (SPEs) are particularly useful due to their disposability, minimum sample preparation, simplicity of the apparatus, obtaining of fast results, cost effectiveness, and lack of requirement of surface pre-treatment. Working with SPEs using cyclic voltammetry (CV), electrochemical impedance spectroscopy (EIS), or amperometry prepares it for point-of-care applications. Personal glucose biosensor used by those suffering from diabetes can be shown as a widespread example of commercialized SPE.

This study is aimed at developing novel enzyme-free sensors for the detection of superoxide radicals in biological samples. For this purpose, ZnO, CuO and CuZn nanoparticles were used in combination with gelatin hydro gel to design the sensors. The requirement of biosensors to have an effective surface area and the catalytic nature of CuZn in the active region of SOD enzyme makes the CuZn multicomponent an excellent candidate for superoxide radical biosensing application. Thus in addition to CuO and ZnO nanoparticles, CuZn nanostructures were also studied as a superoxide radical sensing platform. Designing enzyme-free diagnostic tools makes them economical and biologically durable compared to those including enzymes.

2. Materials and methods

2.1. Materials

Superoxide dismutase (EC. 1.15.1.1, 75KU) from bovine erythrocytes, xanthine oxidase (EC 1.1.3.22, 0.3 U mg^{-1}, from milk), xanthine (2,6-dihydroxypurine) sodium salt, gelatin from porcine bone, glutaraldehyde cross-linking agents, CuZn alloy nanoparticles (150 nm), CuO nanoparticles (<50 nm), ZnO nanoparticles (<50 nm), sodium chloride (NaCl), potassium chloride (KCl), sodium bicarbonate ($NaHCO_3$), potassium ferrocyanide ($K_4[Fe(CN)_6]$), potassiumferricyanide ($K_3[Fe(CN)_6]$), sodium dihydrogenorthophosphate (NaH_2PO_4), and disodium hydrogen orthophosphate (Na_2HPO_4) were purchased from Sigma (St Louis, MO, USA). De-ionized water was purified using a MilliPore Simplicity unit to a resistivity ≥ 18.2 MΩ cm. Electrochemical measurements were carried out with a Gamry Instrument using Framework Version 5.50 software.

2.2. Preparation of biosensors

The polymer was prepared by dissolving in phosphate buffer (0.05 M, pH 7.4) so as to obtain the desired ratio (2%) in the final solution. To prepare the electrodes containing SOD, nanoparticles, glutaraldehyde cross-linking agent and SOD were added to the gelatin containing situated in an eppendorf, respectively (Scheme 1). Homogeneity was provided by vortexing after each addition for a period of 30 s. Next, 2 μL of the mixed solution were added dropwise to the electrode surface. Enzyme-free electrodes were prepared using the same protocol without the enzyme. These modified electrodes were left at room temperature for 2 h to ensure a stable dry surface. Electrochemical measurements were carried out in a 5 mL electrochemical cell. In order to trigger the

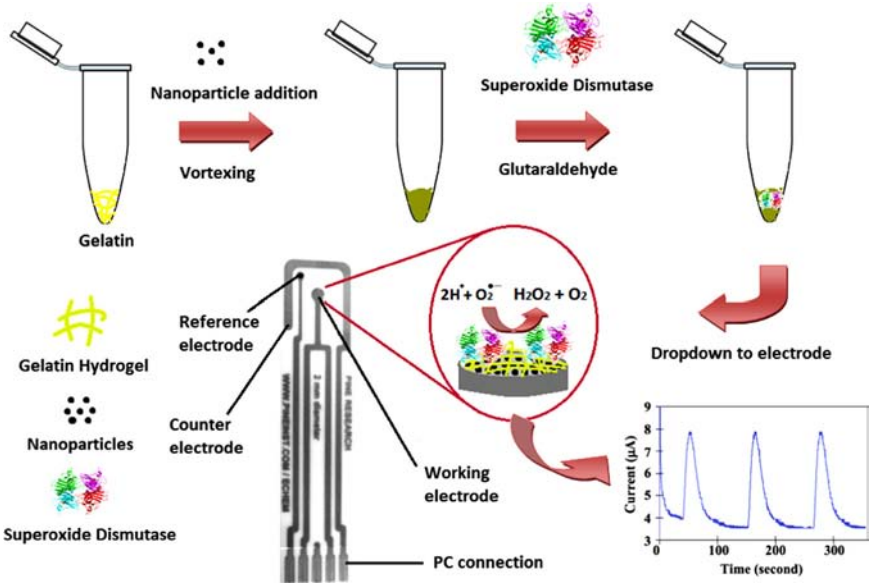

Scheme 1. Schematic presentation and preparation steps of gelatin-nanoparticle-SOD screen-printed electrode. After modification of the platinum SPE electrode with the enzyme and cross-linker containing gelatin solution, amperometric results are obtained with injection of xanthin into xanthin oxidase containing electrochemical cell .

dismutation reaction, the desired concentration of xanthine in 100 μL of buffer was injected into the cell containing 4.9 mL total volume of buffer and xanthine oxidase.

2.3. Electrochemical study

All-in-one platinum screen printed electrodes with a 2 mm diameter working surface, counter and silver reference electrodes were used for the biosensor design. Platinum SPE electrodes were used due to their reusable feature. When the electrodes are electrochemically cleaned and reactivated in sulfuric acid, they can be used over and over again until their surface is destroyed. The other reason that makes SPE electrodes superior is their high stability, durability and conductivity. Printing of platinum on ceramic templates also prevents the electrode system from the adverse effect of acids or bases. A 5 mL volume electrochemical cell for screen-printed electrode was used in all the experiments. CV and EIS were performed in PB buffer containing 0.1 M KCl and 0.5 mM $Fe(CN)_6^{3-/4-}$. Cyclic voltamograms were obtained by cycling the potential between −0.4 and 0.6 V with a scan rate of 100 mVs^{-1}. EIS measurements were recorded within the frequency range of 0.01 Hz to 100 kHz at open circuit potential. All experimental procedures for the development of the biosensors were performed at least three times.

The electron-transfer coefficient and electron-transfer rate constant could be determined based on the Laviron theory (Eqs. (1) and (2)) [31]

$$Epc = E'^0 + \frac{RT}{\alpha snF} - \frac{RT}{\alpha snF} \ln v \quad (1)$$

$$Ep\alpha = E'^0 + \frac{RT}{(1-\alpha s)nF} - \frac{RT}{(1-\alpha s)nF} \ln v \quad (2)$$

where n is the electron transfer number, R is the gas constant (R=8.314 J mol^{-1} K^{-1}), T is the temperature in Kelvin (T=298 K) and F is the Faraday constant (F=96493 C mol^{-1}).

When $n\Delta Ep > 200$ mV, the electron transfer rate ks could be estimated with Laviron's equation (Eq. (3)) [31]

$$ks = \frac{anFn}{RT} \quad (3)$$

The effective surface areas were determined by CV in 0.5 mM $Fe(CN)_6^{3-/4-}$/0.1 M KCl solution in the potential range of −400 to +600 mV. Scan rates of 10, 50, 100, 200, 500, and 1000 mV s^{-1} were employed. The reduction peak current was determined and effective surface areas of electrodes were calculated by the Randles–Sevcik equation (Eq. (4)) as described below

$$i_p = (2.69 \times 10^5) n^{3/2} D^{1/2} C A v^{1/2} \quad (4)$$

where n is the number of transferred electrons for the redox reaction, D is the diffusion coefficient (6.70×10^{-6} cm^2 s^{-1}), C is the molar concentration of ferricyanide (0.5 mM), A is the effective surface area (cm^2), and v is the scan rate (V s^{-1}). The value of n is equal to one for cyclic voltammograms obtained in $Fe(CN)_6^{3-/4-}$, due to the following half reaction taking place at the electrode:

$$Fe(CN)_6^{3-} + e^- \rightarrow Fe(CN)_6^{4-}$$

Graphs using i_p and $v^{1/2}$ were drawn and slopes (k) were calculated. Using the modified Randles–Sevcik equation (Eq. (5)), effective surface areas were calculated

$$A = k/((2.69 \times 10^5) n^{3/2} D^{1/2} C) \quad (5)$$

2.4. Principle of the method

The biosensor used to determine the $O_2^{\bullet -}$ was obtained by coupling an amperometric electrode for hydrogen peroxide with the superoxide dismutase enzyme or nanoparticles immobilized on a gelatin support system. The capacity of the $O_2^{\bullet -}$ biosensor was determined in the following way. The $O_2^{\bullet -}$ is produced in aqueous solution by oxidation of xanthine to uric acid in the presence of xanthine oxidase

$$Xanthine + H_2O + O_2 \xrightarrow{XOD} Uricacid + 2H^+ + O_2^{\bullet -}$$

SOD or CuZn nanoparticles immobilized on the electrode catalyzes the dismutation reaction of the $O_2^{\bullet -}$ releasing oxygen and hydrogenperoxide according to the reaction given below:

$$2H^+ + O_2^{\bullet -} \xrightarrow{SOD} H_2O_2 + O_2$$

The H_2O_2 can be detected at the electrode surface in accordance with the following reaction:

$$H_2O_2 \rightarrow 2H^+ + O_2 + 2e^-$$

The current generated by oxidation of hydrogen peroxide at the working electrode held at 650 mV relative to the Ag/AgCl electrode is proportional to the concentration of $O_2^{\bullet -}$ in solution. Oxidation of H_2O_2 generates the electrons which create a current on the electrode surface which is the principle reaction of superoxide detection. Glucose detection is also dependant on this phenomenon. Our previous experiences have shown that 650 mV is the optimum potential for the oxidation of H_2O_2 in super oxide detection systems [1,32,33].

2.5. Effects of scavengers

The effect of molecules regarded as scavengers for the superoxide radical were determined in vitro using gelatin–CuZn–SOD and gelatin–CuZn electrodes. The response of the electrodes to the superoxide radical both in the presence and absence of scavenger molecules such as acetylsalicylic acid, aspirin, and aspirin containing vitamin C were determined. The selected scavenger molecule (12.5 gL^{-1}) obtained by dissolving and homogenizing the weighed sample in phosphate buffer (0.05 M, pH 7.4) was added to the cell containing phosphate buffer (0.05 M, pH 7.4) and XOD (0.7 U) right before measurement.

2.6. Medical application

The biosensor response was investigated on healthy and cancerous brain tissue, meningioma (grade I, WHO 2000) obtained from Ankara University, Medical School, Oncology Department. The healthy or cancerous brain tissue (0.5 g) was homogenized in distilled water (3 mL) using a Bandalin homogenizer. A solution of the homogenized healthy or cancerous brain tissue (100 μL) was added and the biosensor response recorded. The tissues were stored at −20 °C before use.

3. Results and discussion

3.1. Optimization and characterization of nanobiosensors

3.1.1. Optimization of nanobiosensors

Different parameters affecting the nanobiosensor's performance, namely, the gelatin matrix, glutaraldehyde cross-linker, SOD enzyme, nanoparticles and xanthin oxidase concentrations were investigated and the results have been presented in supplementary materials (Figs. S1–13). Maximum amperometric responses were obtained for a gelatin ratio of 2% with the gelatin–CuO–SOD biosensor. Low gelatin

ratios increased the nanoparticle and/or enzyme leakage due to increased pore size, and smooth film formation was not observed at low polymer concentrations. At higher levels the response increased due to an increase in the amount of nanoparticle/enzyme bondage. Finally, further increase caused decrease of the biosensor response, probably due to excess nanoparticle/enzyme binding, leading to inactivation. Diverse concentrations of cross-linker were used to immobilize SOD onto the carrier systems. Increasing the glutaraldehyde concentration reduced the response of immobilized SOD, due to deactivation of the enzyme molecules and formation of a tight gel structure because of the excess cross-linker. Adversely, the low cross-linker concentration decreased the amperometric signal due to

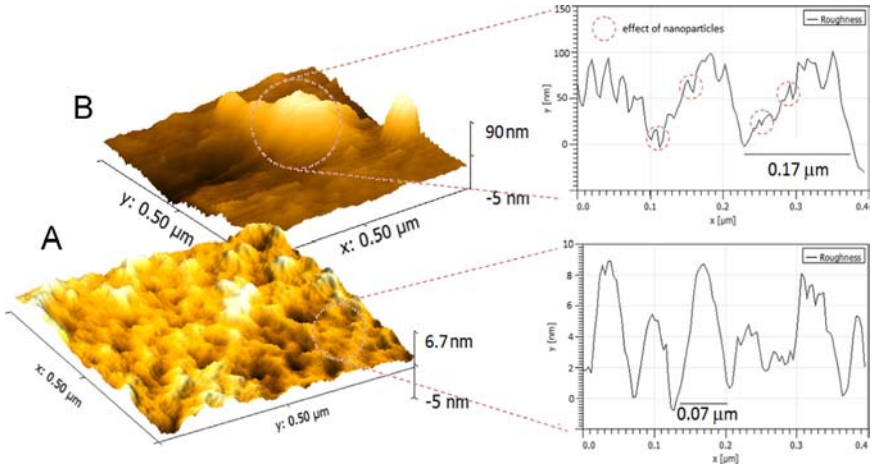

Fig. 1. D Surface topography image of gelatin (A) and roughness graph; and image of gelatin–CuZn–SOD (B) obtained by AFM. Although enzyme incorporation decreases the porosity and active surface area, nanoparticles increase it as presented in the roughness graphs.

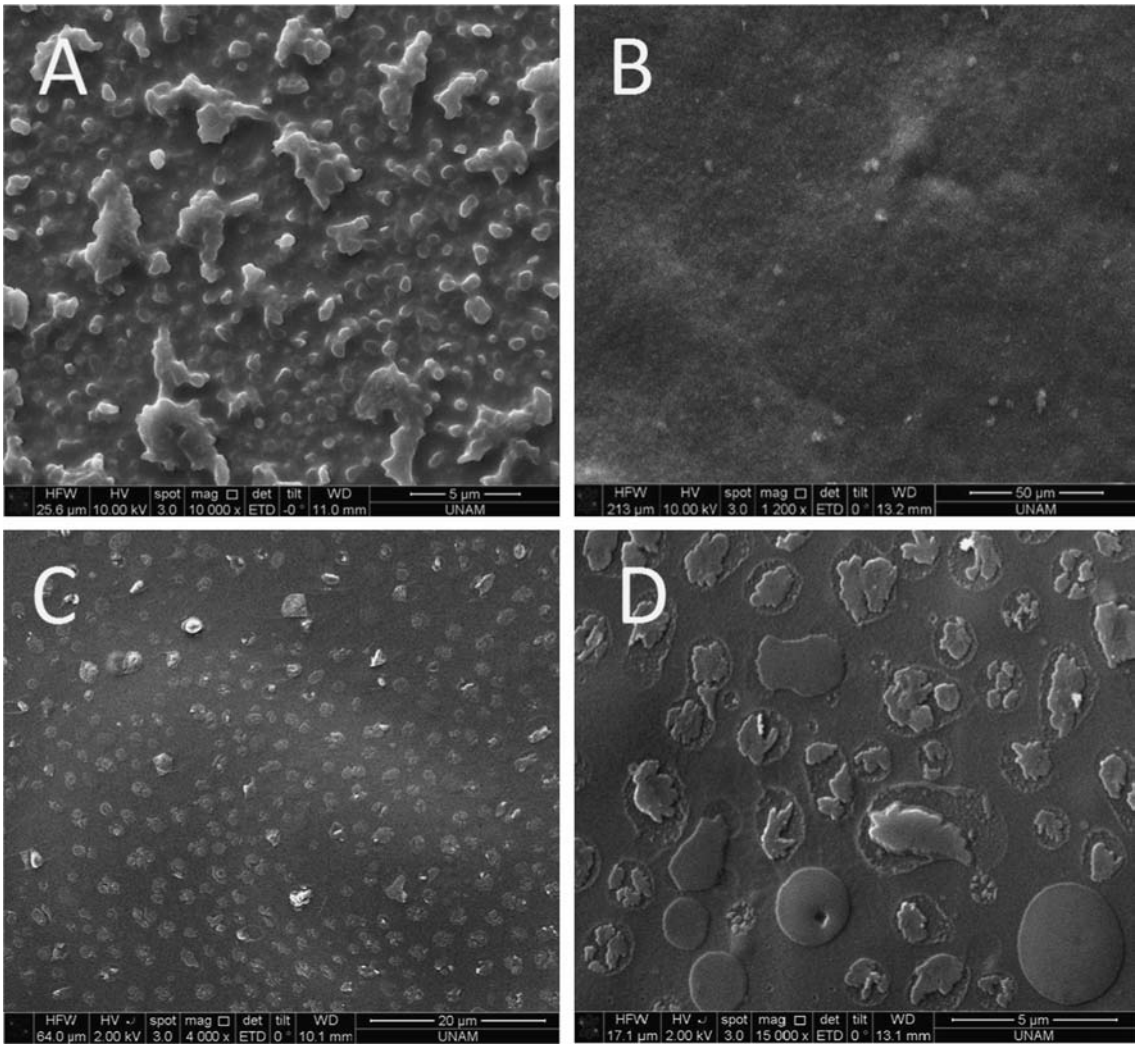

Fig. 2. SEM micrographs of the gelatine (A), gelatine–CuZn nanocomposite (B), gelatine–SOD (C), and gelatine–CuZn–SOD electrode (D).

insufficient immobilization of SOD to gelatin. Optimum concentration of glutaraldehyde was found as 0.0032 M in which the electrodes gave the best results. Many electrodes were prepared using different amounts of nanoparticles for optimization of the nanoparticles' content. The results showed that low nanoparticle levels resulted in low amperometric signals due to insufficient electron transfer. Optimum nanoparticle content was found to be 0.0003 g. Enzyme optimization was performed using different concentrations of SOD where the optimum concentration was found to be 100 U. The amperometric response increased with increasing SOD concentration up to a limit followed by a decrease in the signal. This behavior can be attributed to an increase in enzyme–enzyme cross-linking. In addition, with increased enzyme loading, oversaturation within the matrix pores may have occurred leading to restriction of product and substrate diffusion. Similar results were obtained for xanthine optimization. The same optimum values were obtained for ZnO- and CuZn-based nanobiosensors. Phosphate buffer was chosen as the best reaction environment (Figs. S14–16).

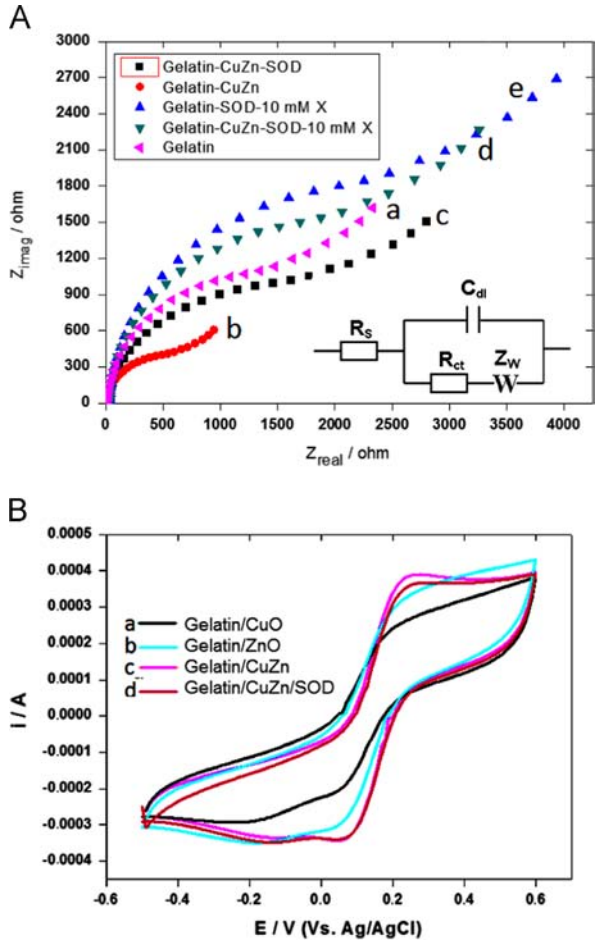

Fig. 3. (A) Nyquist diagram of CuZn-based electrode: (a) gelatin modified electrode; (b) CuZn embedded gelatin electrode; (c) SOD immobilized gelatin–CuZn electrode; (d) 10 mM xanthin injected gelatin–CuZn–SOD electrode; and (e) 10 mM xanthin injected gelatin–SOD electrode. (B) Cyclic voltammograms of gelatin electrodes containing different nanoparticles: (a) CuO embeded gelatin electrode; (b) ZnO embedded gelatin electrode; (c) CuZn embedded gelatin electrode; and (d) SOD immobilized gelatin–CuZn electrode. Solution composition: 0.1 M KCl, 0.5 mM $K_3[Fe(CN)_6]/K_4[Fe(CN)_6]$, pH 7.4. The frequency range 0.01 Hz to 100 kHz at 220 mV open circuit potential. Scan rates 100 mVs^{-1}.

3.1.2. *Surface topography study with AFM and SEM*

Surface topographies of gelatin and gelatin–CuZn–SOD electrodes were investigated with atomic force microscopy (AFM) (Fig. 1). The AFM image of gelatin shows a porous and well settled gelatin carrier surface. Gelatin also covers almost the entire surface enabling an efficient immobilization surface. With enzyme immobilization, the surface roughness of gelatin is seen to decrease although the nanoparticles embedded in the gelatin matrix lead to enormous enzyme dimensions. Though the nanoparticles cannot be seen distinctly in the image, the effect of nanoparticles on the roughness can be seen on the roughness graph. Such a nanoporous rough surface morphology results in an increased effective surface area for enzyme immobilization preventing the leaching of enzymes from the electrode surface.

The gelatine surface is quite rough and not a wholly formed structure as seen from Fig. 2(A). The gelatin CuZn nanocomposite structure on the other hand is relatively smooth and seems to form a complete matrix compared to the gelatin structure (Fig. 2(B)), making it suitable for biosensor studies. The SOD immobilized micrograph given in Fig. 2(C) shows the immobilized enzyme structure. Due to the fact that a hydrogel is used as polymer matrix the embedded nanostructures cannot be seen clearly. But looking at Fig. 2(D) we can see that with the incorporation of enzymes on the surface, due to increasing surface tension, the nanostructure around the enzymes can be seen embedded in the gelatin structure.

Table 2
Electrochemical performance of the electrodes.

Electrode type	ks_a (s^{-1})	α_a	ks_c (s^{-1})	α_c
Gelatin–CuO–SOD	5.84	0.75	1.94	0.25
Gelatin–ZnO–SOD	5.92	0.76	1.86	0.24
Gelatin–CuZn–SOD	6.31	0.81	1.48	0.19
Gelatin–CuZn	6.15	0.79	1.63	0.21

Table 3
Analytical data of the electrodes.

Electrode type	Correlation coefficient	Limit of detection (μM)	Calibration equation
Gelatin–CuO–SOD	0.9965/0.9817	0.89	I/μA=33.68[Xanthin]+0.64 I/μA=1.48[Xanthin]+13.44
Gelatin–ZnO–SOD	0.9932/0.9930	1.64	I/μA=18.19[Xanthin]+2.90 I/μA=1.86[Xanthin]+1.18
Gelatin–CuZn–SOD	0.9533/0.9836	0.31	I/μA=95.62[Xanthin]+1.13 I/μA=2.17[Xanthin]+17.98

Table 1
Linear calibration equations of the electrodes.

Electrode type	LRE (anodic)	LRE (cathodic)
Gelatin–CuO–SOD	$Ip_a/\mu A=(36.78)+(0.82\pm0.04)\nu/mV\ s^{-1}$	$Ip_c/\mu A=-(37.84)\ (0.78\pm0.03)\ \nu/mV\ s^{-1}$
Gelatin–ZnO–SOD	$Ip_a/\mu A=(36.84)+(0.90\pm0.05)\nu/mV\ s^{-1}$	$Ip_c/\mu A=-(32.33)-(0.68\pm0.04)\ \nu/mV\ s^{-1}$
Gelatin–CuZn–SOD	$Ip_a/\mu A=(30.58)+(0.95\pm0.03)\nu/mV\ s^{-1}$	$Ip_c/\mu A=-(83.53)-(1.14\pm0.05)\ \nu/mV\ s^{-1}$
Gelatin–CuZn	$Ip_a/\mu A=(30.03)+(0.69\pm0.02)\nu/mV\ s^{-1}$	$IIp_c/\mu A=-(60.96)-(0.65\pm0.03)\ \nu/mV\ s^{-1}$

LRE is abbreviation of Linear Regression Equation.

3.1.3. Electrochemical study

Electrochemical properties of modified electrodes were evaluated through CV and EIS. EIS is an effective technique for probing the features of surface modified electrodes. The Nyquist plots including real (Z') and imaginary ($-Z''$) parts were obtained, for an equivalent circuit (Fig. 3(A) inset) consisting of solution resistance, double-layer capacitance, charge transfer resistance and Warburg resistance, and used to determine the relative change in surface-charge resistance. The spectra of CuZn electrodes (Fig. 3(A)) consist of a large semicircle (charge transfer) with a straight line (diffusion limited) in low frequency range known as the Warburg element. When the CuZn nanoparticles were embedded in the gelatin hydrogel, surface charge resistance decreased from 2523 Ω to 1196 Ω due to the surface area enhancement of the nanoparticles that enabled low level of target molecule detection. With enzyme immobilization on the gelatin–CuZn nanocarrier platform, the Rct value increased to 2783 Ω giving evidence to immediate surface confinement of SOD. Injecting xanthine to both gelatin–SOD and gelatin–CuZn–SOD electrode drastically increased the electrochemical impedance indicating the proceeding of the dismutation reaction. Similar results were also obtained for the electrodes prepared using CuO and ZnO nanoparticles (Figs. S17 and 18).

Cyclic voltammetry of electro active species, $Fe(CN)_6^{3-/4-}$, is an available tool for evaluating the kinetic barrier of the interface [34]. Fig. 3(B) shows the CV graphs of $Fe(CN)_6^{3-/4-}$ with electrodes including different nanoparticles. The formal potentials ($E_0=(Ep_a+Ep_c)/2$) of the gelatin–CuO, gelatin–ZnO, gelatin–CuZn, and gelatin–CuZn–SOD electrodes are estimated to be 110, 140, 155, and 160 mV vs. Ag/AgCl, respectively. The peak separations (defined as $Ep=Ep_a-Ep_c$) of these electrodes which were determined as 220, 228, 110, and 112 mV, and the asymmetrical nature of the anodic and cathodic peak currents indicate the electron transfer reaction to proceed quasireversibly [35,36]. The graph reveals with immobilization of SOD to the gelatin–CuZn carrier system the electron transfer of $Fe(CN)_6^{3-/4-}$ decreases due to extra resistance created by SOD.

CVs of the gelatin–CuO–SOD, gelatin–ZnO–SOD, gelatin–CuZn–SOD, and enzyme-free gelatin–CuZn electrode at different scan rates were also obtained. The scan rate graphs of the electrodes can be found in Supplementary information (Fig. S19–23). The peak currents were enhanced with the increasing scan rates where both anodic and cathodic peak currents were proportional to the scan rate from 10 to 1000 mV s^{-1}. As seen from Table 1, the linear regression equation indicates the involvement of a surface-controlled quasi-reversible electrochemical process on the electrode.

The plots of the peak potential (Ep_a, Ep_c) vs. the natural logarithm of scan rate (ln ν) for all the electrodes provide information for the calculation of the electron-transfer coefficients (αs) and electron-transfer rate constants (ks). The plots of Ep versus lnυ yielded two straight lines with slopes of $RT/(1-\alpha)nF$ and $-RT/\alpha nF$ for the anodic and cathodic peaks as seen from the graph (Fig. S20). According to Laviron's procedure, from the potential scan rate dependence of the anodic and cathodic peak potentials, the relevant kinetic parameters of the electrodes can be obtained. Therefore, the anodic (ks_a) and cathodic (ks_c) electron transfer rate constants and the anodic (α_a) and cathodic (α_c) transfer coefficients were evaluated using the graphs (Figs. S24–26).

The results show (Table 2) the electron transfer rate constant of the electrode including SOD and CuZn nanoparticles to be higher than that of the other electrodes. The fast electron transfer rate of gelatin–CuZn–SOD electrode might be attributed to the specificity

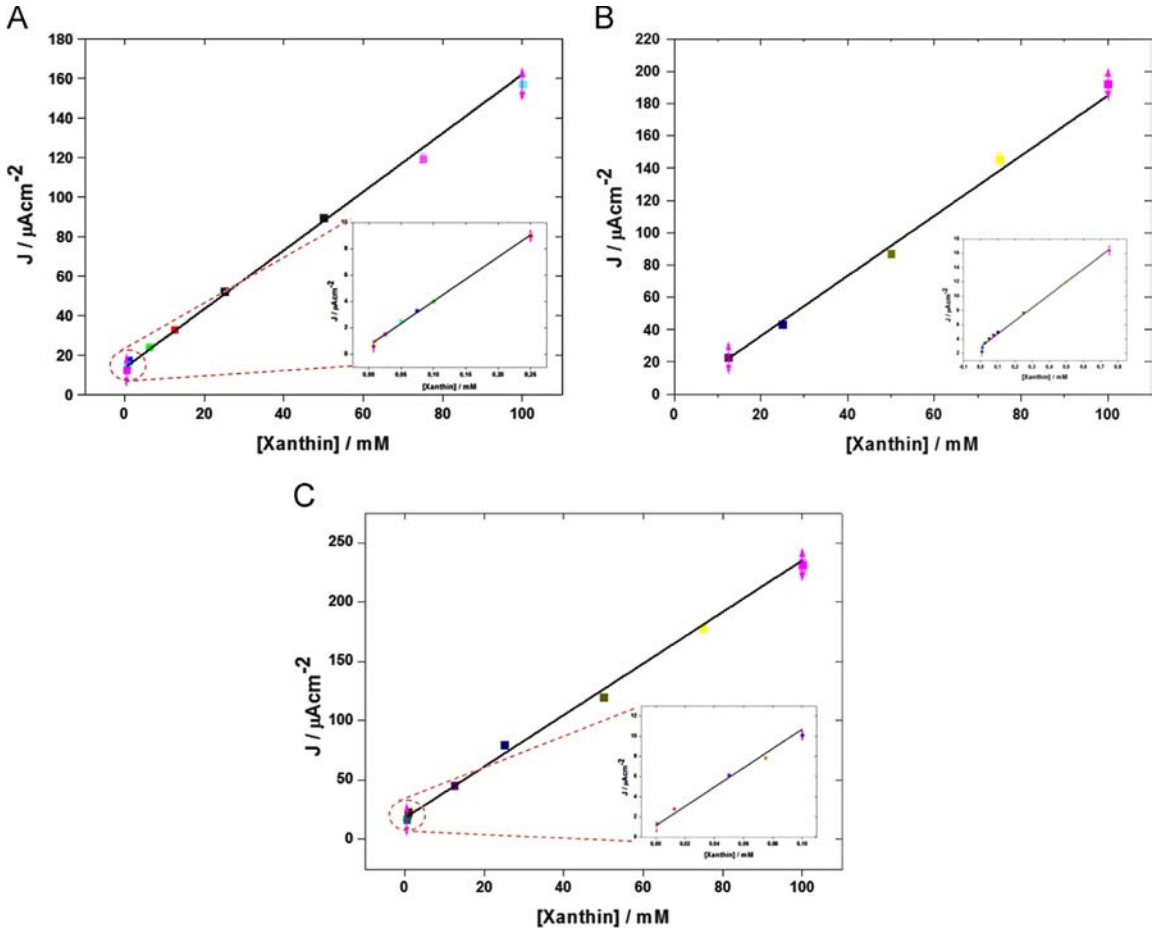

Fig. 4. High and low (inset) concentration range calibration curves of (A) gelatin–CuO–SOD electrode; (B) gelatin–ZnO–SOD electrode; and (C) gelatin–CuZn–SOD electrode.

of the CuZn structure toward the active center of the enzyme. As indicated earlier, the conversion of superoxide anions and protons to peroxide is catalyzed by the SOD enzyme where the active region of SOD, containing the CuZn structure, plays an important role in the process. Incorporation of CuZn alloy nanoparticles on to the sensor platform design should result in enhanced catalysis for the conversion of this reaction. The enzyme-free gelatin–CuZn revealed excellent kinetic performance with respect to the electrodes lacking CuZn nanoparticles. Data obtained from the enzyme-free electrodes prepared with CuO and ZnO have not

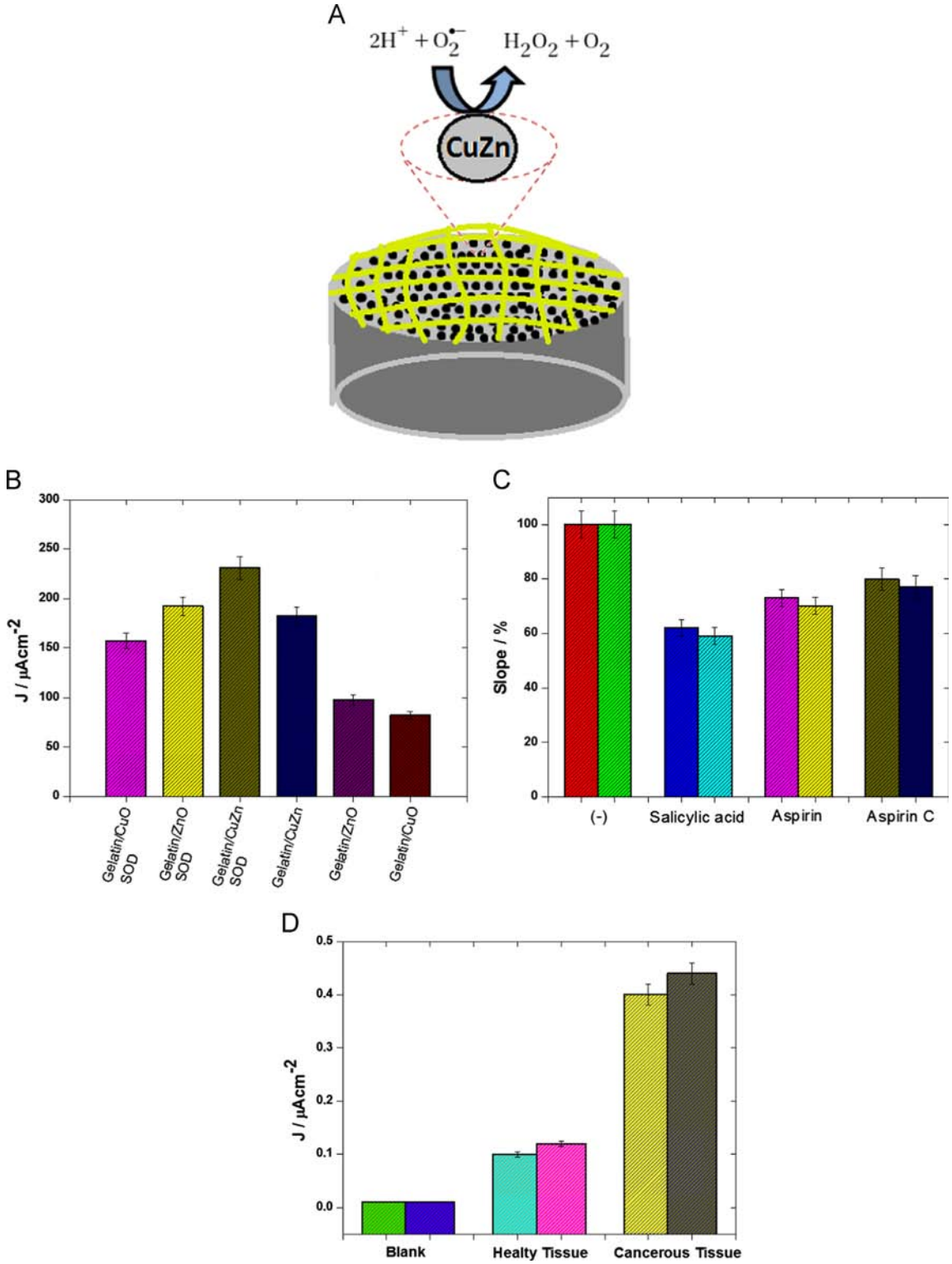

Fig. 5. (A) Schematic illustration of direct catalyzing enzyme-free gelatin–CuZn electrode; (B) comparison of amperometric signals corresponding to 100 mM xanthine obtained by both enzyme containing and enzyme-free electrodes; (C) evaluation of scavenger properties of acetylsalicylic acid-based drugs using the gelatin–CuZn (right side of the columns) and gelatin–CuZn–SOD (left side of the columns) biosensors; and (D) variation of the signal from gelatin–CuZn (left sides of the columns) and gelatin–CuZn–SOD (right sides of the columns) biosensors after addition of homogenized healthy and cancerous brain tissue with phosphate buffer (0.05 mM, pH 7.4). All data are average results from three measurements.

been presented here because of their poor electrochemical and analytical performance

The effective surface areas of the electrodes were also determined using CV, with the aid of the Randles–Sevcik equation [37] where the peak currents (i_p) vs. ln v graphs (Figs. S27–29) were utilized. The results revealed the ZnO embedded electrodes to have a 14.4% higher surface area than CuZn embedded electrodes. This situation can be attributed to high particle size of CuZn alloy nanoparticles (150 nm) compared to CuO and ZnO (<50 nm). The ZnO embedded electrode also has an effective surface area on average 11.1% higher than the CuO embedded electrode, which is thought to be the result of the high isoelectric point of ZnO (8.7–10.3).

3.1.4. Comparison of the developed nanobiosensors with and without enzyme

The amperometric response of the nanobiosensors towards $O_2^{\bullet -}$ was investigated in the buffer solution. A simple and efficient method was used for the generation of $O_2^{\bullet -}$ by oxidation of xanthine to uric acid in the presence of xanthine oxidase at an applied potential of 650 mV. When xanthine is injected into the medium, a superoxide "burst" occurs followed by a rapid decrease to the baseline level due to dismutation. Table 3 shows the main analytical data of the nanobiosensors obtained from the calibration curves (Fig. 4).

The detection limits of the biosensors were calculated as 0.89 μM for gelatin–CuO–SOD, 1.64 μM for gelatin–ZnO–SOD, and 0.31 μM for gelatin–CuZn–SOD electrodes (at a signal-to-noise ratio of 3). Peak intensities of both electrodes, SOD containing electrodes and direct catalyzing enzyme-free electrodes (Fig. 5(A)), were compared using 100 mM of xanthine (Fig. 5(B)). The gelatin–ZnO and gelatin–CuZn electrodes containing SOD gave a more intense peak with respect to the enzyme-free electrodes. On the other hand, the gelatin–CuZn electrode was seen to give a more intense peak in comparison to the gelatin–CuO–SOD electrode. Enzyme-free gelatin–CuO and gelatin–ZnO electrodes were seen to give weak peaks around 35% and 42% compared to the gelatin–CuZn–SOD, which is not functional in designing biosensors. However, the enzyme-free gelatin–CuZn electrode gave a peak of 79% which is lucrative for superoxide radical sensing.

3.1.5. Effect of scavengers

Some molecules and drugs are potential scavengers of superoxide radicals [38,39]. For this purpose, acetylsalicylic acid, Aspirin, and Aspirin C were used and amperometric measurements were carried out using both gelatin–CuZn–SOD and enzyme-free gelatin–CuZn electrodes in the absence and presence of these scavengers (Fig. 5(C)). The antioxidant properties of the scavenger molecules tested were evaluated from the percentage ratio of the slope values of the calibration plot of the gelatin–CuZn–SOD electrode (Fig. 4(B)). Addition of salycylic acid, aspirin and aspirin C samples decreased the signal strengths as the antioxidant species reacted with the superoxide radical, thus reducing its concentration in the solution. There was a consequent decrease in the amount of H_2O_2 released and as a result in the amperometric signal. It can be deduced that pure salycylic acid has a more intense scavenger effect. Hence the developed biosensor can also be used for in vitro determination of antioxidant properties of salicylic acid-based drugs.

3.1.6. Medical application

The biosensor response was also tested on healthy and cancerous brain tissue (Fig. 5(D)) using both gelatin–CuZn–SOD and enzyme-free gelatin–CuZn electrode. Different signals were obtained from the biosensor depending on whether the tissue was healthy or cancerous. Cancerous brain tissue contains higher quantities of superoxide radicals compared to a healthy tissue. This is probably due to smaller quantities of scavenger molecules or endogenous SOD being present in the cancerous tissue. The values obtained by both electrodes were seen to be fairly close to each other, indicating the viability of the enzyme-free electrode for clinical analysis of superoxide radicals.

4. Conclusion

Technology has always been an indispensable part in the development of biosensors. The performance of biosensors is being strongly improved using new materials such as nanoparticles or other smart materials. The use of nanoparticles in biosensor technology allows innovation in designing more sensitive, economical, rapid, easy-to-use, and lab-on-chip type diagnostic systems. In recent years, enzyme-free catalyzing of some redox reactions have become trendy. Therefore the designability of sensors for the determination of superoxide radicals was investigated in this study. The results obtained from the enzyme-free sensors were hopeful but not as advanced as those from the biosensor containing enzyme. The gelatin–CuZn enzyme-free sensor showed an electrochemical performance of 80% compared to the enzyme containing electrode. On the other hand, the enzyme-free sensors prepared with CuO and ZnO nanoparticles did not show the same advanced performance. It seems that the detection of superoxide radicals will be feasible using enzyme-free sensors in biological samples with further advanced studies.

Acknowledgments

This work is financially supported by the Scientific and Technological Research Council of Turkey (no. 113S255).

Appendix A. Supporting information

Supplementary data associated with this article can be found in the online version at http://dx.doi.org/10.1016/j.talanta.2014.11.003.

References

[1] O. Kocabay, E. Emregul, S. Aras, K.C. Emregul, Bioprocess. Biosyst. Eng. 35 (6) (2012) 923–930.
[2] R.S. Sohal, B.H. Sohal, W.C. Orr, Free Radical Biol. Med. 19 (1995) 499–504.
[3] R. Misiaszek, C. Crean, A. Joffe, N.E. Geacintov, V. Shafirovich, J. Biol.Chem. 279 (2004) 32106–32115.
[4] J.R. Woods, Placenta 22 (2001) S38–S44.
[5] S. Mak, G.E. Newton, Chest 120 (2001) 2035–2046.
[6] P. Kovacic, J.D. Jacintho, Curr. Med. Chem. 8 (2001) 773–796.
[7] B.E. Leonard, Int. J. Dev. Neurosci. 19 (2001) 305–312.
[8] I. Fridovich, Acc. Chem. Res. 5 (1972) 321.
[9] I. Fridovich, J. Biol. Chem. 272 (1997) 18515.
[10] A. Okado-Matsumoto, I. Fridovich, J. Biol. Chem. 276 (2001) 38388.
[11] L.A. Sturtz, K. Diekert, L.T. Jensen, R. Lill, V.C. Culotta, J. Biol. Chem. 276 (2001) 38084.
[12] J.S. Valentine, P.A. Doucette, S.Z. Potter, Annu. Rev. Biochem. 74 (2005) 563–593.
[13] B.K. Beissenhirtz, F.W. Scheller, M.S. Viezzoli, F. Lisdat, Anal. Chem. 78 (3) (2006) 928–935.
[14] K. Prasad, J. Kalra, B. Bhardwaj, J. Exp. Pathol. 70 (1989) 463.
[15] J. Vasquez-Vivar, N. Hogg, K.A. Pritchard, B. Kalyanaraman, FEBS Lett. 403 (1997) 130.
[16] T. Ohyashiki, M. Nunomura, T. Katoh, Biochim. Biophys. Acta 1421 (1992) 139.
[17] T. Oshaka, Y. Shintane, F. Matsumoto, T. Okajima, K. Tokuda, Bioelectrochem. Bioenerg. 37 (1995) 73.
[18] K. Tammeveski, T.T. Tenno, A.A. Mashirin, E.W. Hillhouse, P. Manning, C. J. McNeil, Free Radic. Res. Commun. 25 (1998) 973.
[19] K. Tanaka, Y. Muto, Bioelectrochem. Bioenerg. 29 (1992) 143.
[20] S. Luo, F. Su, C. Liu, J. Li, R. Liu, Y. Xiao, Y. Li, X. Liu, Q. Cai, Talanta 86 (2011) 157–163.

[21] S. Anandan, X.-G. Wen, S.-H. Yang, Mater. Chem. Phys. 93 (2005) 35.
[22] Z.-L. Jin, X.-J. Zhang, Y.-X. Li, S.-B. Li, G.-X. Lu, Catal. Commun. 8 (2008) 1267.
[23] S.F. Zheng, J.S. Hu, L.S. Zhong, W.G. Song, L.J. Wan, Chem. Mater. 20 (2008) 3617.
[24] N.Q. Dung, D. Patil, H. Jung, D. Kim, Biosens. Bioelectron. 42 (2013) 280–286.
[25] Z.-J. Zhuang, X.-D. Su, H.-Y. Yuan, Q. Sun, D. Xiao, M. Choi, Analyst 133 (2008) 126.
[26] X. Wang, C.-G. Hu, H. Liu, G.-J. Du, X.-S. He, Y. Xi, Sens. Actuators B: Chem. 144 (2010) 220.
[27] A. Umar, M.M. Rahman, A. Al-Hajry, Y.B. Hahn, Electrochem. Commun. 11 (2009) 278.
[28] J. Liu, X. Huang, Y. Li, K.M. Sulieman, X. He, F. Sun, Cryst. Growth Des. 6 (2006) 16901.
[29] M. Ahmad, C. Pan, L. Gan, Z. Nawaz, J. Zhu, J. Phys. Chem. C 17 (2010) 243–250.
[30] P. Norouzi, V.K. Gupta, F. Faridbod, M. Pirali-Hamedani, B. Larijani, M. R. Ganjali, Anal. Chem. 83 (2011) 1564–1570.
[31] E. Laviron, J. Electroanal. Chem. 101 (1979) 19–28.
[32] E. Emregul, O. Kocabay, B. Derkus, T. Yumak, K.C. Emregul, A. Sinag, K. Polat, Bioelectrochemistry 90 (2013) 8–17.
[33] E. Emregul, Anal. Bioanal. Chem. 383 (6) (2005) 947–954.
[34] B. Rezaei, N. Majidi, H. Rahmani, T. Khayamian, Biosens. Bioelectron. 26 (2011) 2130–2134.
[35] Z. Deng, Q. Rui, X. Yin, H. Liu, Y. Tian, Anal. Chem. 80 (2008) 5839–5846.
[36] H. Liu, Y. Tian, P. Xia, Langmuir 24 (2008) 6359–6366.
[37] J. Shi, J.C. Claussen, E.S. McLamore, A. Haque, D. Jaroch, A.R. Diggs, P. Calvo-Marzal, J.L. Rickus, D.M. Porterfield, Nanotechnology 22 (2011) 355502.
[38] B.N. Ames, R. Cathcart, E. Schwiers,and, P. Hochstein, Proc. Natl. Acad. Sci. USA 78 (1981) 6858.
[39] A. Nandi, I.B. Chatterjee, J. Biosci. 11 (1–4) (1987) 435–441.